CHANGES IN THE RAMAN AND FLUORESCENCE SPECTROSCOPIC SIGNATURES OF IRRADIATED ORGANIC-MINERAL MIXTURES: IMPLICATIONS FOR MOLECULAR BIOSIGNATURE DETECTION ON MARS. A. C. Fox[1], R. S. Jakubek[2] and J. L. Eigenbrode[3], [1]NASA Postdoctoral Program – NASA Johnson Space Center Houston, TX, USA, [2]Jacobs, NASA Johnson Space Center, Houston, TX 77058, [3]Solar System Exploration Division, NASA Goddard Space Flight Center, Greenbelt, MD, USA.

Introduction: The lack of a global magnetic field and relatively thin atmosphere on Mars provide little shielding from the galactic cosmic rays and solar energetic particles. These particles are energetic enough to penetrate several meters into the Martian surface, potentially altering and/or destroying organic material preserved in the geologic record (1). Despite this hostile radiation environment, organic compounds and bulk organic matter have been detected in the shallow subsurface (< 10 cm) at several locations on Mars (2-7). To understand the origins of these organics, it is critical to constrain how their potentially diagnostic molecular features have been altered by ionizing radiation. Here, we studied diverse organic materials exposed to high-energy protons for cumulative radiation doses up to 500 kGy and characterized by a deep UV Raman and fluorescence instrument analogous to the Scanning Habitable Environments with Raman & Luminescence for Organics & Chemicals (SHERLOC) instrument onboard the Mars 2020 Perseverance Rover (8). Previous investigations of these samples revealed the formation of organic acids as metastable radiolysis products (9), indicating either complete or partial breakdown of the initial organic material. The focus of the current work was to further characterize these samples by identifying other radiolysis products using techniques comparable to the Mars 2020 Perseverance SHERLOC instrument.

Methods & Materials: Mineral matrices included fused silica (SiO_2) and a synthetic analog mixture composed of 50% nontronite (Nau-1, The Clay Mineral Society; $Na_{0.3}Fe_2(Si,Al)_4O_{10}(OH)_2{\cdot}nH_2O$) and 50% olivine sand ($(Fe, Mg)_2SiO_4$). Organic material was chosen to represent a range of chemical states of sedimentary organic matter found in the terrestrial record. In order of increasing maturity, organic material included either 50 ppm of a standard solution of individual organic compounds, 5 wt% Pony Lake fulvic acid (International Humic Substances Society), or 5 wt% of an Archean kerogen isolate. The standard solution of individual organics, referred as organic mix, consisted of 50 ppm by weight for each of pristane, phytane, sterane, *n*-heptadecane, stigmasterol, pyrene, phenanthrene, C14:0 fatty acid, C18:1 fatty acid, l-alanine, l-serine, glycine, mellitic acid, benzoic acid, and adipic acid. Organic-mineral mixtures were packed in an ashed quartz-glass cuvette and purged under 99.999% Ar prior to irradiation with 200 MeV protons. Samples received cumulative doses of either 0, 63, 125, 250, or 500 kGy. Raman and fluorescence measurements were collected on the Analogue Complimentary Raman for Operations oN Mars (ACRONM) instrument, an analogue to the SHERLOC instrument.

Results: *Fluorescence Results.* In the macromolecular organics (kerogen and fulvic acid) and fused silica samples two broad fluorescence peaks were observed at ~295 and ~395 nm. The fused silica and organic mix samples similarly had a feature at 295 nm and several overlapping peaks in the 390 – 460 nm region. Exposure to ionizing radiation caused the lower wavenumber feature, 295 nm, to blue-shift to ~280 nm and became more narrow and more intense with increasing radiation in all samples. In contrast, the higher wavenumber features in all samples showed decreasing intensity with increasing radiation dose.

Significant changes in the fluorescence profiles of the synthetic analog samples were not observed. The kerogen and synthetic analog samples had a prominent band centered at 309 nm and a relatively weak band centered around 425 nm. Neither feature showed a consistent trend with increasing radiation, but the peak area and height for the 309 nm feature were significantly larger for the irradiated samples compared to the non-irradiated sample. The synthetic analog and organic mix samples had a feature centered at 428 nm that did not change with radiation dose.

Raman Results. For the fused silica and synthetic analog samples, Raman features associated with organic compounds were detected in the 1300 – 1700 cm^{-1} range. In the kerogen and fulvic acid samples, we observed a G band generally located in the 1580 – 1605 cm^{-1} and no D band was observed. For fused silica and kerogen samples, the G band shows a modest decrease in peak height and decrease in peak position with increasing radiation. In contrast, the G band was only detectable in the non-irradiated fused silica and fulvic acid samples, with a band centered at 1604 cm^{-1} and after radiation exposure, organic features are not detectable. For the synthetic analog and kerogen samples, there was a slight decrease in peak area and height with increasing radiation. We observed an increase in peak position with increasing radiation,

which was the opposite trend observed in the fused silica samples.

In the fused silica and organic mix samples, several peaks were observed in the 1340 – 1620 cm^{-1} range. With exposure to radiation, the peak area and height decreased until no organic-associated peaks were visible at 500 kGy.

Discussion: Exposure to ionizing radiation resulted in both the formation and destruction of organic material in the organic-mineral mixtures. The fluorescent feature observed at 280/295 nm in the fused silica samples increased in peak height and area with increasing radiation (Fig. 1) is consistent with the formation of an organic radiolysis product. This product is likely some type of single ring aromatic species (i.e., benzene), which fluoresce in the 270 – 330 nm region (10).

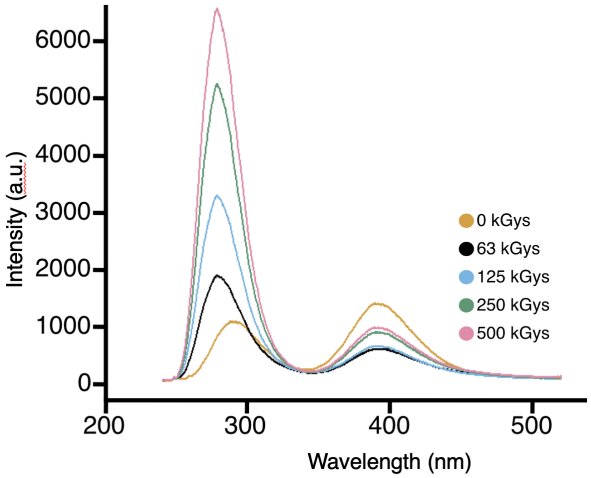

Fig 1. Representative fluorescence spectra of the fused silica and kerogen samples (8).

In contrast, other fluorescent and Raman features decreased in peak height and area with increasing radiation, indicating the breakdown of organic material. Organic degradation was sensitive to both the type of organic material and mineral matrix.

Macromolecules displayed a higher resistance to radiolysis than individual organic molecules, with kerogen persisting at the highest radiation dose compared to the complete loss of organic Raman features in the organic mix sample at 500 kGys. This result suggests that the structure of kerogen is playing a protective role against ionizing radiation.

Opposing changes in the G band peak properties of the kerogen samples suggest that the radiolysis of organic material is influenced by mineralogy. The fused silica samples showed a decreasing G band position with increasing radiation, indicating increased polymerization, while the synthetic analog samples showed an increasing G band peak position, indicating the breakdown of aromatic domains (Fig 2). The observed decrease of aromatic domain size suggests that the synthetic analog mineral matrix enhances the radiolysis of kerogen.

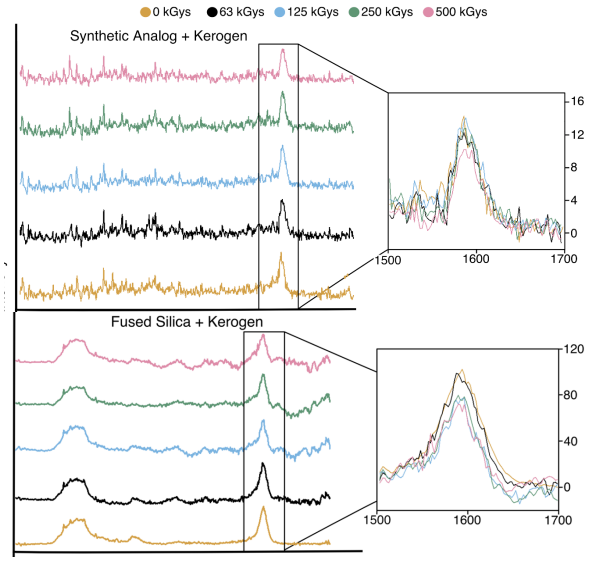

Fig 2. Raman spectra of kerogen samples with G band highlighted (8).

Conclusion: We found that exposure to high energy protons produced a single-ring aromatic radiolysis product in the fused silica samples. The destruction of primary organic material was also observed in all samples at all radiation doses. The available experimental observations suggest that irradiated organic material in sediments will not retain primary molecular features diagnostic of their origins on geologic timescales without additional protective mechanisms. Resistance to radiolysis can be enhanced in macromolecular structures relative to individual compounds, and therefore kerogen-like organic species may provide the best opportunity for evaluating primary molecular features in high radiation environments.

References: [1] Hassler D. M. et al. (2014) *Science*, 343, 1-7. [2] Eigenbrode J. L. et al. (2018) *Science*, 360, 1096-1101. [3] Scheller E. L. et al. (2022) *Science*, 378, 1106-1110. [4] Freissinet, C. et al. (2015) *JGR Planets*, 120(3). [5] Millan, M. et al. (2022) *Nature Astron.* 6 (1), 129-140. [6] Millan, M. et al. (2022) *JGR Planets*, 127 (11). [7] Stern, J. C. et al. (2022) *PNAS*, 119 (27), e2201139119. [8] Fox A. C. et al. (in review) *JGR Planets*. [9] Fox A. C. et al. (2019) *JGR: Planets,* 124, 3257-3266. [10] Bhartia et al. (2008) *Applied Spectroscopy*, 62, 1070-1077.